PERGAMON

Journal of Structural Geology 22 (2000) 1713–1722

JOURNAL OF STRUCTURAL GEOLOGY

www.elsevier.nl/locate/jstrugeo

Crystallographic preferred orientation development by dissolution–precipitation creep

Paul D. Bons[a,*], Bas den Brok[b]

[a]*Tektonophysik, Institut für Geowissenschaften, Universität Mainz, D-55099 Mainz, Germany*
[b]*Geologisches Institut ETH, Strukturgeologie und Tektonik, Sonneggstrasse 5, CH 8092 Zürich, Switzerland*

Received 1 December 1999; accepted 30 May 2000

Abstract

Crystallographic preferred orientations (CPOs) in deformed rocks are commonly interpreted as resulting from crystal plastic deformation mechanisms, where deformation is achieved by the movement of dislocations. In this paper we investigate the possibility of CPO-development by dissolution–precipitation creep or pressure solution. A numerical model is presented, which simulates the development of a grain aggregate that deforms by reaction-controlled dissolution–precipitation creep. Grains are simulated as rectangular boxes that change their shape by growth, or dissolution of their surfaces, depending on the normal stresses acting on the individual surfaces. Grains can also rotate due to an applied vorticity (for non-coaxial deformation) and if they have a non-equidimensional shape. For each strain increment, stress that is applied to the grains is the same for all grains, while individual grains deform and rotate by different amounts. A variety of CPOs develop at moderate strains, depending on the reaction rates of the different crystal-surfaces and type of deformation (uni-axial shortening, plane strain pure shear and simple shear). The modelling results confirm that dissolution–precipitation creep may play a role in CPO-development in rocks.

1. Introduction

Crystallographic preferred orientations (CPOs) are very common in rocks deformed ductily in nature. In structural geology they are used as a tool, for example, to determine whether strain was coaxial or non-coaxial, to determine the sense of shear, the amount of strain, the temperature during deformation, or to obtain information about deformation mechanisms active during their formation (e.g. Law, 1990; Passchier and Trouw, 1996 p. 95). Commonly, the presence of a CPO is interpreted as evidence for deformation by dislocation creep (e.g. Hobbs et al., 1976; Wenk, 1985; Knipe, 1989) and, amongst the microstructural indicators for dislocation creep (including undulose extinction, subgrains, recrystallised grains, and a high free dislocation density), the presence of a CPO is the only indicator for a significant contribution of dislocation creep, as the other microstructures may already develop with only very low dislocation creep strains.

Another significant deformation mechanism in rocks is dissolution–precipitation creep (DPC). Here, differential stresses induce dissolution at some sites and precipitation at other sites, which leads to a change of shape of a rock volume: i.e. strain (e.g. Rutter, 1976). Equant grains, grain indentations, overgrowths and a lack of a CPO are generally quoted as characteristic microstructures for DPC (Knipe 1989).

However, CPOs are also reported to have developed in quartz rocks in which some form of DPC was the dominant deformation mechanism and it was argued that these CPOs were due to crystallographic orientation-dependent dissolution and growth of quartz grains (Hippertt, 1994; Stallard and Shelley, 1995; Takeshita and Hara, 1998). Evidence that such orientation dependent dissolution and/or growth can occur in rocks is presented by Becker (1995) for naturally deformed quartz rocks, by den Brok (1992, 1996) for experimentally deformed quartz rocks and by Heidelbach et al. (2000) for experimentally deformed albite aggregates.

If DPC can lead to development of CPOs, then the presence of a CPO on itself cannot be used as an argument for deformation by dislocation creep. One needs to be able to distinguish between CPOs that are characteristic for DPC and CPOs that are characteristic for dislocation creep. To this end, Tullis (1989) modelled CPO-development by DPC assuming crystallographically controlled anisotropy in the rates of dissolution and growth under non-hydrostatic stress. In the present paper, a numerical

* Corresponding author. Fax: +49-6131-3923863.
E-mail address: bons@mail.uni-mainz.de (P.D. Bons).

0191-8141/00/$ - see front matter
PII: S0191-8141(00)00075-4

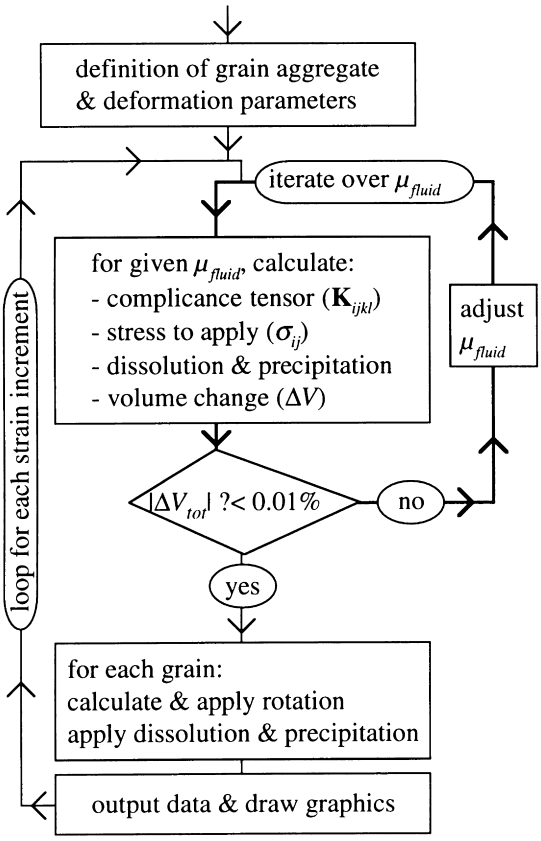

Fig. 1. Flow chart of the numerical model, showing the sequence of routines, which are described in the text. The program contains two main loops: (i) an iteration loop (bold line) to determine μ_{fluid} and the compliance tensor **K**, embedded in (ii) a loop for each small strain increment.

simulation of CPO development by DPC based on the crystallographically controlled anisotropy in the rates of dissolution and growth is presented. The aim of the study is to find out, firstly, whether DPC can lead to significant CPOs and, secondly, what types of CPOs are expected to develop.

2. Theoretical background and numerical model

Dissolution–precipitation creep is commonly believed to be driven by gradients in grain boundary surface normal stress (τ) and there is general agreement that the stress-induced differences in thermodynamic chemical potential ($\Delta\mu$) of the solid in the grain boundary solution is approximately proportional to the differences in normal stresses acting on the grain surfaces, $\Delta\tau$ (e.g. Paterson, 1973; Lehner, 1990):

$$\Delta\mu \propto \Delta\tau \tag{1}$$

Under an applied differential stress, equilibrium potentials will be different from site to site within a grain aggregate as they depend on τ acting on differently oriented grain boundaries. Dissolution and precipitation strive to achieve local chemical equilibrium between the grain boundary surfaces and adjacent solution, leading to variations in solute concentration (C). Diffusion counteracts this process, and the effect is dissolution at grain boundaries with a relatively high τ and diffusional transport of the solute to grain boundaries with a relatively low τ, where precipitation can take place.

If the diffusion process is slow and rate controlling (Shimizu, 1995), C is close to equilibrium with respect to the stressed solid everywhere throughout the entire aggregate. If the dissolution and/or precipitation process is slow and rate controlling, C is approximately the same everywhere, and generally not in equilibrium with respect to the solid under stress. Dissolution and precipitation rates for a given $\Delta\mu$ vary significantly with crystallographic orientation of the crystal face for most minerals. So, if dissolution and/or precipitation is rate controlling, DPC could, in principle, lead to the development of a CPO (Tullis, 1989). This is the hypothetical mechanism of CPO formation that is explored in the numerical model described below. It simulates deformation of a grain aggregate by dissolution–precipitation rate controlled DPC and calculates the lattice orientation of each grain in the grain aggregate during progressive deformation in small strain increments. A flow chart of the computer model is given in Fig. 1.

2.1. Definition of the grain aggregate

The model does not simulate any particular mineral. Instead, for mathematical simplicity, a numerical mineral analogue is used that has a tetragonal symmetry with three perpendicular axes (Fig. 2). Only grain surfaces perpendicular to these axes are allowed, which implies that all grains have rectangular box-shapes at all times. One of the axes is denoted as the 'A-axis' and is perpendicular to the 'basal plane', while the two other axes are denoted as 'B-axes', perpendicular to the 'prismatic planes'. In the simulations presented here, 750 grains were created at the start of each simulation. In all cases the number of grains decreases during a run. Although the total volume of the aggregate is kept nearly constant, individual grains may loose or gain volume, and some grains eventually disappear completely. Since no nucleation is included in the model, this means that the total number of grains decreases and the average grain size increases.

Each grain is given a random orientation. The lengths of the crystals parallel to each axis are initially randomly set within a range of a factor two, which means that the maximum axial ratio of the grains is two. The average grain size at the start is set to unity and initial sizes thus range from 0.25 to 2. It is not possible to create a closely fitting aggregate of rectangular grains. Deformation of each grain is treated individually, as if the grain is embedded in a matrix made up of the bulk aggregate (a 'homogeneous equivalent medium'). This approach is similar to the self-consistent approach (e.g. Cleary et al., 1980). Grains, therefore, have no fixed position in space or relative to other grains. Grains

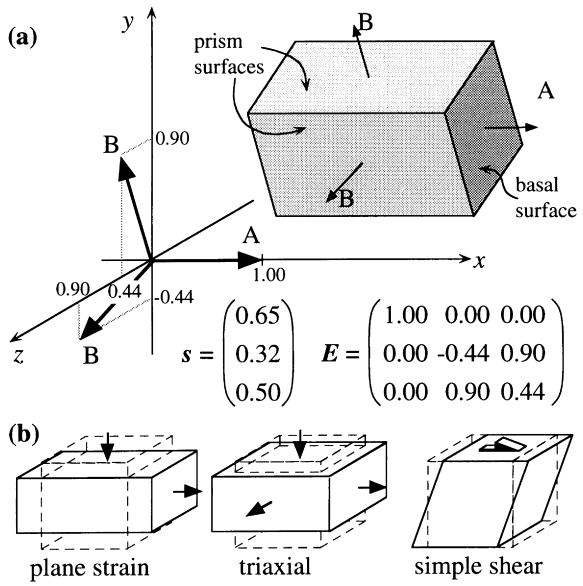

Fig. 2. (a) Definition of grain crystallographic axes and planes of the box-shaped 'mineral'. The axes of this particular grain are shown relative to the global *x*-*y*-*z*-reference frame, as well as the values of the shape vector (***s***) and the orientation tensor (***E***). (b) Three deformation geometries used in the modelling, shown relative to the reference frame of (a): plane strain with shortening along *y*-axis and extension along *x*-axis, triaxial shortening along *y*-axis and outflow in *xz*-plane and simple shear in *x*-direction and *xz* shear plane.

are envisaged to be embedded in a connected grain boundary fluid, which contains dissolved grain material.

The shape and orientation of a grain are expressed by a vector ***s*** with three components that represent the lengths of the grain parallel to the crystallographic axes and a 3×3 tensor ***E***, which contains three unit-vectors parallel to the crystallographic axes, each defined by their *x*-, *y*- and *z*-component in a fixed global reference frame (Fig. 2a). We use standard indicial notation for vectors and tensors, where indices *i, j, k* and *l* each can have values from 1 to 3, representing the three dimensions of Cartesian space (Mase, 1970).

2.2. Deformation parameters

Deformation is calculated for a constant strain rate for the whole aggregate. Most texture models (e.g. Jessell, 1988) assume strain compatibility at the cost of violating stress compatibility. In our case, stress is assumed to be the same everywhere within the aggregate, while each grain deforms at a different rate. Strain compatibility is thus violated. Each grain is assumed to be embedded in an equivalent homogeneous medium in which it can deform freely according to the imposed stress.

Different deformation geometries can be imposed on the aggregate, and we only present simulations for volume conservative: (i) triaxial shortening; (ii) plane strain pure shear; and (iii) dextral simple shear (Fig. 2b). Deformation is calculated for small strain increments, typically 1% shortening for coaxial deformation and a shear strain of 0.02 to 0.04 for simple shear.

2.3. Dissolution and precipitation at grain boundaries

To calculate the amount of dissolution and precipitation at the grain boundaries, we choose a model where dissolution and precipitation control the deformation rate simultaneously. This means that the driving force for dissolution and/or growth is the difference between the thermodynamic potential (μ_i) of the solid in solution at an interface perpendicular to the *i*-th axis of a grain, and some average potential (μ_{fluid}) of solid in solution, assumed to be equal everywhere throughout the aggregate. The rate ($\partial s_i/\partial t$) at which grains dissolve and/or grow, expressed as the rate of change of the half-length of the grain in the direction of *i*-th axis of the grain, is then proportional to the crystallographic orientation dependent dissolution/precipitation rate (P_i) per unit driving force perpendicular the *i*-th axis of the grain multiplied by the driving force ($\mu_{\text{fluid}} - \mu_i$):

$$\partial s_i/\partial t \propto P_i(\mu_{\text{fluid}} - \mu_i) \tag{2}$$

The thermodynamic potential for a grain face normal to *i* (μ_i) is proportional to the normal stress (τ_i) acting on that face (Eq. 1), which in turn is related to the stress state, defined by the deviatoric stress tensor σ in the global reference frame:

$$\mu_i \propto \tau_i = \sigma_{kl} \cdot \mathbf{E}_{ik} \cdot \mathbf{E}_{il} \tag{3}$$

By inserting Eq. (3) in Eq. (2) and replacing ∂t by Δt for a small finite time increment, we obtain the equation for the new half lengths of a grain after time increment ∂t:

$$s_{i,t=t+\Delta t} = s_{i,t=t} + P_i(\mu_{\text{fluid}} - \sigma_{kl} \cdot \mathbf{E}_{ik} \cdot \mathbf{E}_{il}) \cdot \Delta t \tag{4}$$

All parameters in Eq. (4) are known or set by the user, except μ_{fluid}, which is not known *a priori*. μ_{fluid} is chosen such that the total volume of the grains does not change (i.e., the aggregate is taken as a closed system in which total dissolution equals total precipitation). This value for μ_{fluid} can be determined iteratively for each deformation step. Since μ_{fluid} may change during deformation, the actual total amount of solid and dissolved grain material may change as well. The actual amount of fluid is, however, never stated and is effectively assumed to be infinitesimally small compared to the volume of the solid grains. Once μ_{fluid} is determined, the changes in lengths along the axes of all grains can be calculated and applied by changing the vector ***s*** for each grain.

Each grain deforms by a different amount, with the strain rate tensor, $\dot{e}^*$, for each grain in a reference frame parallel to the grain axes given by:

$$\dot{e}^*_{ii} = \frac{s_{i,t=t+\Delta t} - s_{i,t}}{\Delta t} = \frac{\Delta s_i}{\Delta t} \;\&\; \dot{e}^*_{i \neq j} = 0 \tag{5}$$

The strain rate in the global reference frame, $\dot{e}$, is given

by:

$$\dot{e}_{kl} = \frac{\Delta s_i}{\Delta t} \cdot E_{ik} \cdot E_{il} \tag{6}$$

Each grain contributes a different amount to the total strain rate of the aggregate. The strain rate of the whole aggregate in the global reference frame, $\dot{\varepsilon}$, is the volume-weighed sum of the strain rates of the N individual grains, each with volume $V_{(n)}$:

$$\dot{\varepsilon}_{ij} = \sum_{n=1}^{N} V_{(n)} \dot{e}_{ij(n)} \Big/ \sum_{n=1}^{N} V_{(n)} \tag{7}$$

2.4. Rotation of grains

Grains not only change their shape, but may also rotate in a deforming aggregate. There are two causes for rotation: (i) vorticity induced rotation and (ii) shape-controlled rotation of non-equidimensional grains due to deformation of the surrounding matrix. Both vorticity-induced and shape-controlled rotation only modify the orientation tensor **E** for each grain.

In the model, deformation is achieved by applying a stress tensor to the aggregate. This stress-tensor is by definition symmetric, i.e. essentially coaxial. Any non-coaxial deformation is achieved by adding a bulk rigid body rotation. For instance, to achieve horizontal simple shear, plane strain pure shear is applied at 45° to the shear plane and then the appropriate bulk rotation is applied to obtain simple shear. Since grains do not have a recorded position in space, this vorticity induced bulk rotation is equivalent to a simple rigid body rotation of all grains around the vorticity axis in the global reference frame.

Grains are rigid in the model, as they can only change their shape by dissolution and precipitation on their surfaces. During deformation rigid grains are expected to rotate, depending on their shape. During coaxial deformation, equidimensional grains are not expected to rotate, but elongate grains tend to rotate towards fabric attractors (Jeffery, 1922; Passchier, 1987, 1997). During non-coaxial deformation, even equidimensional grains may rotate. The rotation of an individual grain in a natural aggregate is influenced by the configuration and behaviour of its neighbours. This is, however, not known in the model. We therefore use the Jeffery (1922) model of a single rigid inclusion in a homogeneous linear viscous matrix as an approximation and neglect interactions between individual grains. ten Brink (1996) showed that low axial ratio box-shaped inclusions closely follow the predicted rotation behaviour of ellipsoids with the same axial ratio. We then used the equations of Jezek (1994) for rotation of ellipsoidal inclusions.

The strain rate of the matrix is the same as the set strain rate of the whole aggregate: the equivalent homogeneous medium. Since vorticity-induced rotation is treated separately, only the coaxial component of the applied strain rate tensor is used to calculate and apply the rotation of a single grain. To do so, we first express the matrix strain rate ($\dot{\varepsilon}$) in the reference frame parallel to the axes of that grain, using:

$$\dot{\varepsilon}^*_{ij} = \dot{\varepsilon}_{ij} \cdot E_{ik} \cdot E_{jl} \tag{8}$$

The rotation rates around the three axes of the grain ($\dot{\omega}_i$ around the i-th axis) are now given by (Jezek, 1994):

$$\dot{\omega}_1 = \frac{s_3^2 \cdot \dot{\varepsilon}^*_{23} - s_2^2 \cdot \dot{\varepsilon}^*_{32}}{s_2^2 + s_3^2}, \qquad \dot{\omega}_2 = \frac{s_3^2 \cdot \dot{\varepsilon}^*_{13} - s_1^2 \cdot \dot{\varepsilon}^*_{31}}{s_1^2 + s_3^2},$$
$$\dot{\omega}_3 = \frac{s_2^2 \cdot \dot{\varepsilon}^*_{12} - s_1^2 \cdot \dot{\varepsilon}^*_{21}}{s_1^2 + s_2^2} \tag{9}$$

For the given time step Δt, the grain is then rotated over the finite angles $\dot{\omega}_i \cdot \Delta t$.

2.5. Determining the applied stress tensor

A constant strain increment is applied each time interval. However, to achieve this strain increment, a stress tensor needs to be applied to the aggregate. As the aggregate evolves, this stress tensor changes and must therefore be determined for every time interval. Since the aggregate becomes mechanically anisotropic if a CPO develops, we must use a 4-th order compliance tensor (**K**) to describe the relationship between stress and strain rate:

$$\sigma_{ij} = \mathbf{K}_{ijkl} \cdot \dot{\varepsilon}_{kl} \tag{10a}$$

$$\Leftrightarrow$$

$$\dot{\varepsilon}_{kl} = \mathbf{K}^{-1}_{ijkl} \cdot \sigma_{ij} \tag{10b}$$

A complication is that **K**, which has at the most 36 independent components, has to be determined for each strain increment. First, the inverse of **K**, $\mathbf{K}^{-1}$, is determined by in turn applying six different stress tensors to the aggregate, which produce six different strain rate tensors. The different stress tensors are chosen such that the 36 components can be obtained from Eq. (10b). $\mathbf{K}^{-1}$ is then inverted to obtain **K**, with which the desired stress tensor can be calculated with Eq. (10a). This routine only gives an approximation of **K**, as **K** is a function of μ_{fluid}, the average chemical potential of dissolved grain material in the fluid. In addition, the appropriate μ_{fluid} which produces no volume change of the solid is different for different stresses. Within the iteration loop to determine μ_{fluid}, **K** is determined for a given μ_{fluid}, and from that, the stress tensor. This stress is then applied to the whole aggregate and the change in volume is determined. If the volume changes, μ_{fluid} is changed and the routine repeated, until volume change is within $\pm 0.01\%$ (a compromise between calculation speed and accuracy).

As **K** is an approximation, the resulting strain increment is also only an approximation (usually within $\pm 1\%$). After many strain increments this could lead to significant deviation from the desired finite strain. Each strain increment is therefore adjusted to correct for deviations that developed in

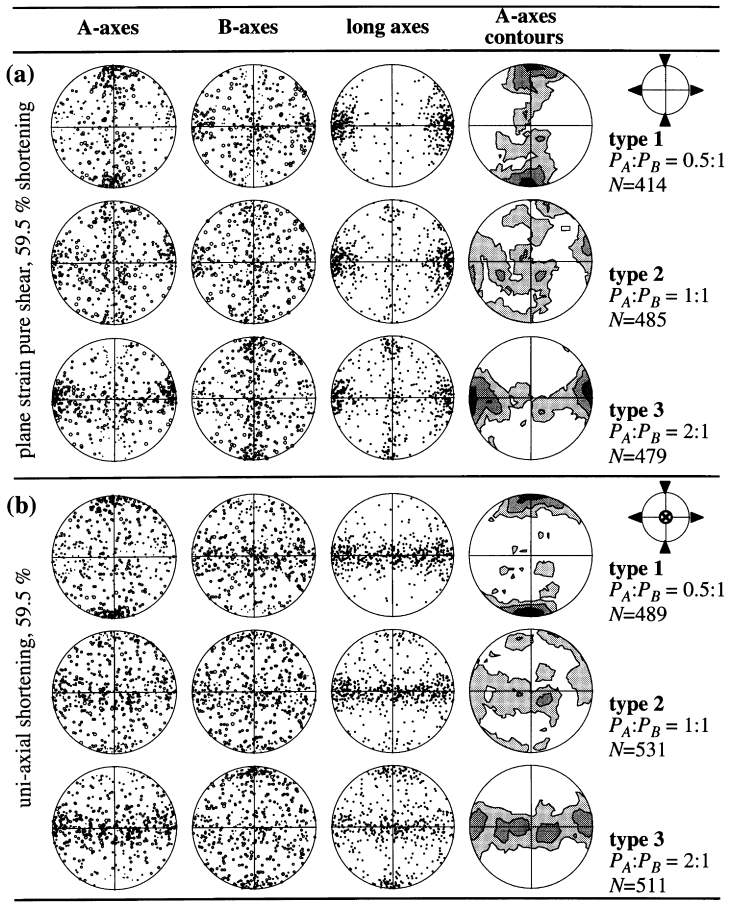

Fig. 3. Modelling results for coaxial deformation to 59.5% shortening after 90 strain increments. (a) Plane strain with N–S shortening and EW extension. (b) Uniaxial N–S shortening. Equal area lower-hemisphere plots of A- and B-axes are shown in the left two columns and long axes of grains in the third column. Dot-size in left two columns is proportional to grain size. The right-most column shows contour plots of the A-axes, contoured at 2% of data per 2% area intervals in equal area projection. For each deformation type, simulations are shown for reaction-symmetry types 1, 2 and 3. In all cases, the total number of grains (N) is smaller than the initial 750, due to selective grain growth.

previous strain increments. Normally this keeps deviations from the desired finite strain within approximately a few percent. However, if only few grains are left and the crystallographic preferred orientation is very strong the numerical system may become unstable and may sometimes collapse.

3. Modelling results

3.1. Crystallographic preferred orientations

Three reaction rate types were simulated with the dissolution/precipitation reaction on the basal surface set to (1) half, (2) equal and (3) double that of the prismatic surfaces. It should be noted that reaction rate type 2 is the most symmetric of the three types, but is not isotropic. Fig. 3 shows the A-axes distribution for 59.5% triaxial shortening and plane strain shortening after 90 strain increments. Reaction rate types 1 and 3 both give strong CPOs for both strain types. Notice that for type 2 the A- and B-axes are interchangeable and therefore both A- and B-axis distributions are the same and are weaker hybrids of type 1 and 3 CPOs. In all cases most grains become aligned with their slow reaction surfaces normal to maximum shortening and fast reaction surfaces normal to maximum extension. For example, reaction rate type 1 gives A-axes point maxima parallel to the shortening direction (y-axis) in both plane strain and triaxial shortening. The B-axes form point-maxima parallel to the extension direction (x-axis) in plane strain shortening and a girdle parallel to the outflow plane (xz-plane). A similar pattern is observed in dextral simple shear simulations (Fig. 4). Girdles initially develop at 45° to the shear direction and then rotate synthetically towards the shear direction (reaction rate type 3) or towards the perpendicular to the shear plane (reaction rate type 1). The initial girdles eventually break down into two point maxima. The more isotropic reaction rate type 2 produces a weaker hybrid CPO of two perpendicular great circles.

The CPOs develop by two main mechanisms: rotation of grains and disappearance of grains. This can be seen in Fig. 5a (reaction rate type 1, simple shear). Grains initially rotate

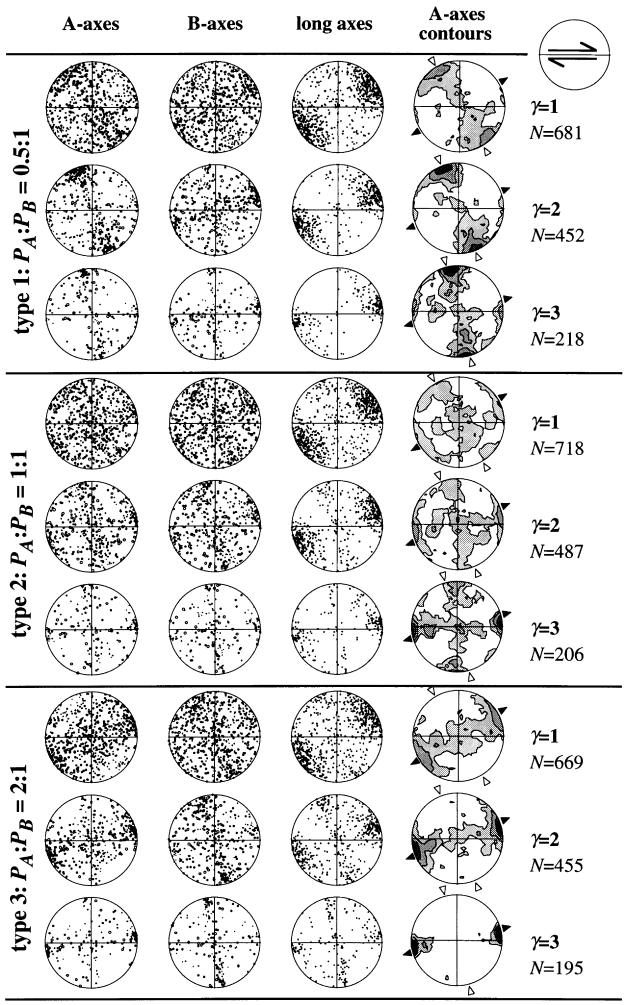

Fig. 4. Results of dextral simple shear simulations (to a shear strain of $\gamma = 3$) in lower-hemisphere equal area plots. First and second columns show A- and B-axes, respectively. Dot size is proportional to grain size. Third column shows the distribution of grain long axes. Fourth column shows contour plots of the A-axes, contoured at 2% of data per 2% area intervals. Triangles show the directions of maximum finite extension (black) and shortening (white). The three reaction-symmetry types 1, 2 and 3 are shown at the top, middle and bottom, respectively. N is the number of grains (starting at 750).

over large angles and only a small proportion of grains disappears. After some strain and development of an initial CPO, complete dissolution of unfavourably oriented grains becomes more important. In the example, a strong CPO is developed after a shear strain of two. This CPO then breaks down as more than 50% of the grains disappear between a shear strain of two and three.

Fig. 5b shows the strongly changing stress needed to keep a constant dextral simple shear rate. At the beginning, the sample is isotropic and only the shear stress (σ_{xy}) is non-zero. Other stress components become non-zero as anisotropy develops with increasing CPO strength. Stresses increase gradually with increasing shear strain, which is also due to the increase in grain size. If stresses are normalised to the starting grain size (Fig. 5c), the shear stress remains approximately constant ($\pm 10\%$), as well as σ_{zz}, while σ_{xx} and σ_{yy} keep changing.

3.2. Shape preferred orientations

Plots of the distribution of the long axes of grains in Figs. 3 and 4 show a preferred orientation in the direction of maximum finite elongation, although reaction rate type 3, and to a lesser extent type 2, also have a girdle perpendicular to the shear direction. Individual grain shapes are, however, highly variable (Fig. 6). The largest grains generally have a low axial ratio or tend towards either prolate or oblate shapes in the plane strain simulations. These results suggest that measurement of average grain shape in thin section may give a good indication of the direction of finite extension, but would underestimate the finite strain.

3.3. Dissolution or precipitation control

Dissolution and precipitation rates for a given plane were equal in the simulations presented above. It is possible in the numerical model to set dissolution and precipitation rates (P_i in Eq. (2)) at different values. To illustrate the effect of this we present simple shear simulations (Fig. 7) for relatively slow precipitation (precipitation rate/dissolution rate = 1/5) and relatively slow dissolution (precipitation rate/dissolution rate = 5/1). The first case approximates precipitation as the rate controlling step and the second dissolution control. Dissolution control gives the strongest CPOs for all reaction rate types, whereas precipitation control gives weaker and more irregular, but more realistic looking CPOs.

4. Discussion

4.1. Comparison with natural CPOs

The modelling results show that CPOs can develop by dissolution–precipitation creep at geologically reasonable strains ($\gamma = 1$–3), provided that DPC is in some way affected by crystallographically controlled anisotropy in dissolution and growth rates of individual grains. It appears that crystallographic directions with *slow* dissolution and growth rates end up in orientations facing the maximum finite shortening direction, and that crystallographic directions with *fast* dissolution and growth rates end up facing maximum extension directions. This is the same as was found by Tullis (1989) and was also proposed by Hippertt (1994) and Stallard and Shelley (1995) as an explanation for the CPOs they observed.

The numerical mineral analogues that were used (types 1, 2 and 3) do not exactly match any particular natural mineral, but the variations in the dissolution and growth rates are realistic (e.g. Sunagawa, 1987; Becker 1995). For example, model material type 3 would approximate quartz, where

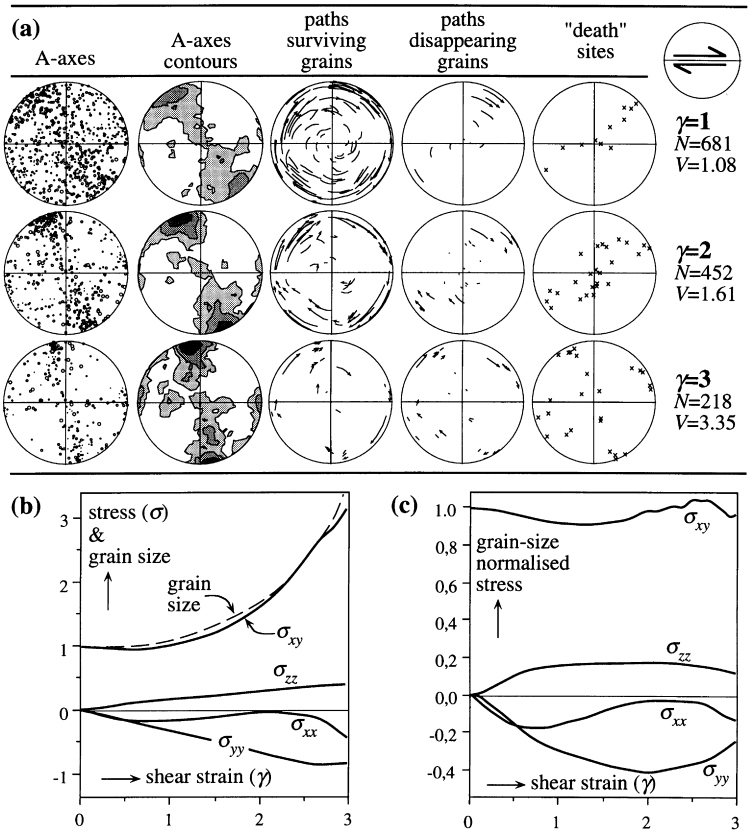

Fig. 5. (a) Illustration of the evolving contribution of grain rotation and selective grain growth to CPO-development, for a dextral simple shear simulation of the symmetry type 1 model mineral. Left column shows A-axes in equal area plots at $\gamma = 1$, 2 and 3. Dot size is proportional to grain size. Second column shows contour plots of the A-axes, contoured at 2% of data per 2% area intervals. The third and fourth columns show A-axes paths for shear strain increments $\Delta\gamma = 0$ to 1, 1 to 2 and 2 to 3. For clarity, only the first 100 grains in the list are shown, with in the third column those grains that survive the whole strain increment and in the fourth those grains that disappear during the given strain increment. The fifth column shows the orientation of A-axis of grains at the moment of complete dissolution ('death') during the given strain increment. *N* is number of grains, starting at 750 and *V* the average grain size, starting at one. (b) Graph of the applied stresses as a function of shear strain (γ). The stresses are normalised to one for the shear stress (σ_{xy}) at the start of the simulation. (c) Graph of the applied stresses, divided by the grain size, as a function of shear strain. This graph shows that the increase in shear stress is mostly due to an increase in grain size.

growth and dissolution parallel to the <c> axis is roughly about two times faster than growth and dissolution perpendicular to <c>, even though the actual anisotropy in growth and dissolution rate of quartz is much more complex, with singular minima in rhombohedral (r) directions and rounded maxima at about 10 to 20° to <c> (Fig. 5 in Chernov and Dimitrov, 1989). In fact, the results on type 3 material for plane strain and pure shear are strikingly similar to the flattening quartz *c*-axis fabrics of Hippertt (1994) and Takeshita and Hara (1998). Model material type 1 would be an analogue of mica and produces *c*-axis point maxima parallel to the direction of maximum finite shortening. Model material type 2 forms an intermediate case between type 1 and 3. Although the growth/dissolution rates of all three facets are the same, it should not be confused with an isotropic material. Growth/dissolution can only take place on the three perpendicular facets and CPOs result from preferred alignment of these facets perpendicular to the principle axes of finite strain. The CPOs are hybrids of those produced by model material type 1 and 3.

4.2. Numerical model limitations and possibilities

It has already been mentioned above that the reaction anisotropy is only a first approximation of realistic reaction anisotropies. Using realistic anisotropies with grains that are multi-faceted or general-shaped polyhedra is theoretically possible, but would greatly increase the complexity of the calculations in the model as the shape and volume of each grain cannot any more be derived from a single vector (***s***) that represents the lengths of the three principle axes of a box-shaped grain.

Probably the most significant limitation to the model is the lack of any recrystallisation mechanism. Jessell (1988) showed that adding recrystallisation to the classical Taylor–Bishop–Hill theory for lattice rotation by dislocation creep significantly changes CPO development. In our model, any process other than stress-induced precipitation or dissolution on grain surfaces is absent. Breaking of grains, grain nucleation and grain boundary migration may all modify the CPO development (Jessell, 1988; Law, 1990; Takeshita and

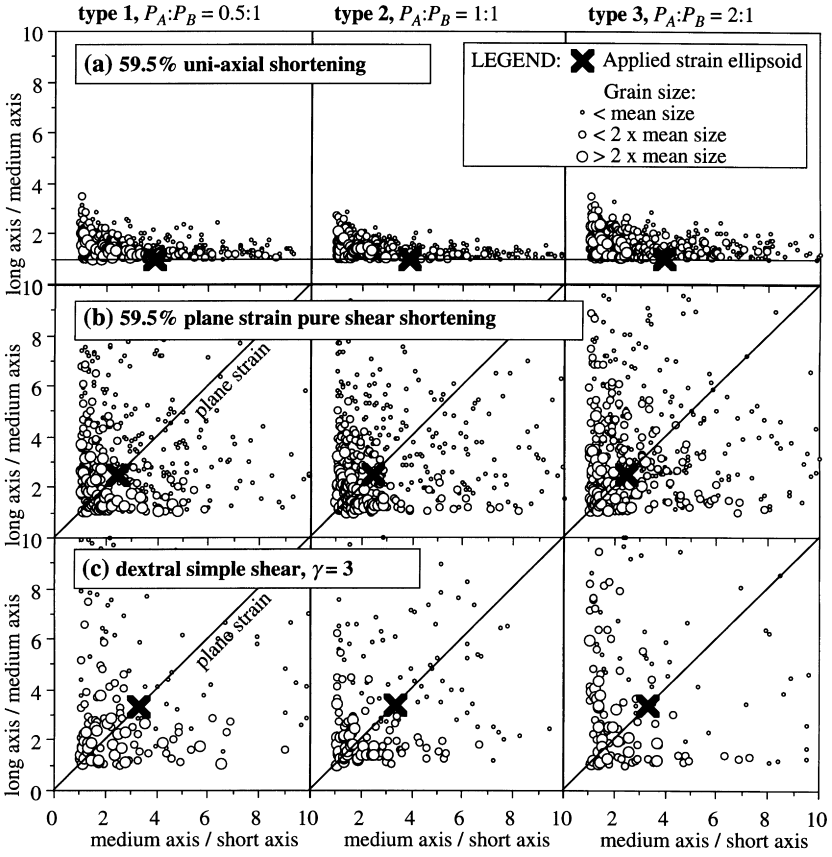

Fig. 6. Flinn diagrams of grain shapes for (a) 59.5% uniaxial shortening, (b) 59.5% plane strain pure shear and (c) simple shear to a shear strain of 3, for reaction-symmetry types 1 (left column), 2 (middle column) and 3 (right column). Dot shape is proportional to grain size. The applied strain ellipsoid for each case is shown with a cross. Notice the strong variation in grain shapes and mostly low axial ratios of the largest grains, while smallest grains can have more extreme axial ratios. In the plane strain cases, grains have a tendency towards either prolate or oblate shapes.

Hara, 1998). An artefact of the lack of these processes is the steadily increasing grain size as more and more grains dissolve completely and no mechanism is included to create new grains. The increasing stresses shown in Fig. 5 are therefore not realistic, but should not be disregarded. More importantly, the relative changes in the stresses show the increasing mechanical anisotropy that is a result of the CPO-development.

However, in this paper we are only concerned with the question whether CPOs would develop during reaction-controlled DPC and rigid body rotation of individual grains. The inclusion of rigid body rotation in the model

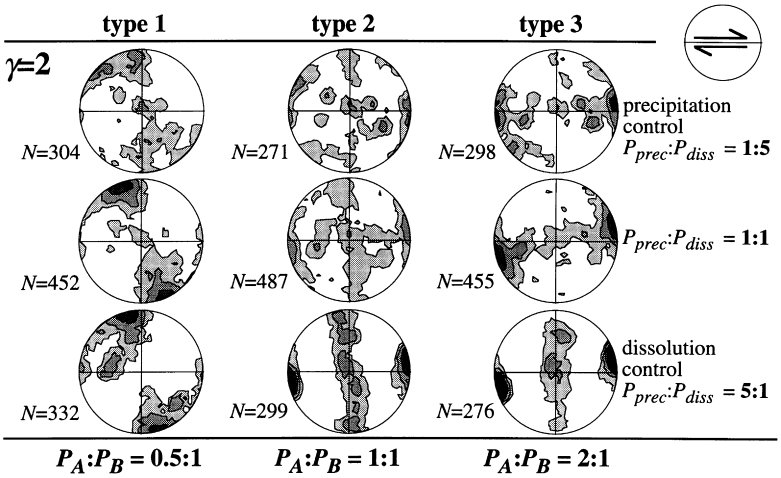

Fig. 7. Results of dextral simple shear simulations ($\gamma = 2$) in lower-hemisphere equal area plots, for the three symmetry types (columns) and for different relative rates of dissolution (P_{diss}) and precipitation (P_{prec}) (rows).

is important, as it plays a significant role in the CPO development (Stallard and Shelley, 1995). However, the freedom given in to model for grains to rotate independently probably overestimates the role of rigid body rotation in the development of CPOs.

The actual DPC mechanisms active in nature are not well understood yet (Spiers and Takeshita, 1995), although dissolution–precipitation creep is considered to be an important deformation mechanism at low metamorphic grade conditions (Groshong, 1988; Harrison and Onasch, 2000). Different DPC models have been proposed, apart from the reaction-controlled DPC assumed in our model.

The relationship between crystallographic orientation and growth/dissolution rates is different for each DPC-mechanism. Each DPC-mechanisms may therefore produce specific types of CPOs. For example, in one group of DPC-mechanisms, the rate-controlling process is diffusion (e.g. Rutter, 1976). In this case, the total amount of material that is transported away from a grain boundary under high normal stress is commonly assumed to be controlled by the diffusivity and the average surface normal stress. The grains on either side of the grain boundary may contribute to a different degree to producing this amount of material that is transported away. CPOs are expected to develop if the amount of contributed material for each grain is related to the crystallographic orientation of these surfaces. This may, for instance, be caused by crystallographically controlled differences in: (i) elastic strain energy (Gal and Nur, 1998); (ii) crystal plastic deformation (Bosworth, 1981); or (iii) microcrack density (Gratz, 1991; den Brok, 1998; Gratier et al., 1999). These mechanisms, however, cannot be modelled by our numerical model, since the assumption of the reaction as the rate controlling step is essential to it.

In all model runs presented here, we have used as one boundary condition that the volume of the grain aggregate remains constant. This condition is not always fulfilled in nature, where DPC may commonly lead to volume changes, as for instance measured by Harrison and Onasch (2000). Any desired rate of volume change can be modelled by changing μ_{fluid}. This possibility of the model has, however, not been explored for this paper, where we have restricted ourselves to only three volume conservative deformation geometries.

5. Conclusions

The first aim of this study was to explore whether or not dissolution-precipitation creep (DPC) could, in principle, produce CPOs at geologically reasonable strains ($\gamma = 1–3$). Modelling of reaction-controlled (i.e. relatively fast diffusion) DPC of model minerals with anisotropic reaction kinetics, in combination with grain rigid body rotation, resulted in a variety of CPOs, some of which are comparable to CPOs found in nature. This implies that the presence of CPOs in deformed rocks is not necessarily evidence for dislocation creep.

In our modelling, CPOs developed by the coupled action of preferential growth or dissolution of grains with certain crystallographic orientations and rigid body rotation of grains. Modelling should therefore include both processes, although the complete freedom of grains to rotate may have overestimated the role of rigid body rotation in our model.

We only modelled one of the various proposed possible DPC mechanisms. This study highlights the need to: (i) clarify which mechanisms actually operate in nature; and (ii) to determine the values of the various parameters that play a role in these mechanisms, such as dissolution and growth rates of mineral faces under geological conditions. Even without such data, our modelling provides an avenue to at least qualitatively explore the often disregarded link between DPC and CPO-development.

Acknowledgements

We thank Mark Jessell and Terence Barr for their help with the programming and critical discussions and João Hippertt and Dave Prior for their reviews.

References

Becker, A., 1995. Quartz pressure solution: influence of crystallographic orientation. Journal of Structural Geology 17, 1395–1405.

Bosworth, W., 1981. Strain-induced preferential dissolution of halite. Tectonophysics 78, 509–525.

ten Brink, C.E., 1996. Development of porphyroclast geometries during non-coaxial flow, Geologica Ultraiectina 142. Ph.D. thesis, Utrecht University.

den Brok, S.W.J., 1992. An experimental investigation into the effect of water on the flow of quartzite. Geologica Ultraiectina 95. Ph.D. thesis, Utrecht University.

den Brok, S.W.J., 1996. The effect of crystallographic orientation on pressure solution in quartzite. Journal of Structural Geology 18, 859–860.

den Brok, S.W.J., 1998. Effect of microcracking on pressure-solution strain rate: The Gratz grain boundary model. Geology 26, 915–918.

Chernov, A.A., Dimitrov, V.S., 1989. Interface between dislocations and cellular front of crystallization: (0001)SiO_2 face. Journal of Crystal Growth 96, 304–315.

Cleary, M.P., Chen, I.W., Lee, S.M., 1980. Self-consistent techniques for heterogeneous media. Journal of Engineering, Mechanics Division 106, 861–887.

Gal, D., Nur, A., 1998. Elastic strain energy as a control in the evolution of asymmetric pressure-solution contacts. Geology 26, 663–665.

Gratier, J.-P, Renard, F., Labaume, P., 1999. How pressure solution creep and fracturing process interact in the upper crust to make it behave in both a brittle and viscous manner. Journal of Structural Geology 21, 1189–1198.

Gratz, A.J., 1991. Solution-transfer compaction of quartzites: progress towards a rate law. Geology 19, 901–904.

Groshong, R.H., 1988. Low-temperature deformation mechanisms and their interpretation. Geological Society of America Bulletin 100, 1329–1360.

Harrison, M.J., Onasch, C.M., 2000. Quantitative assessment of low-temperature deformation mechanisms in a folded quartz arenite, Valley and Ridge Province, West Virginia. Tectonophysics 317, 73–91.

Heidelbach, F., Post, A.D., Tullis, J., 2000. Crystallographic preferred orientation in albite samples deformed experimentally by dislocation and solution precipitation creep, Journal of Structural Geology (this volume).

Hippertt, J.F., 1994. Microstructures and c-axis fabrics indicative of quartz dissolution in sheared quartzites and phyllonites. Tectonophysics 229, 141–163.

Hobbs, B.E., Means, W.D., Williams, P.F., 1976. An outline of Structural Geology. John Wiley and Sons, New York.

Jeffery, G.B., 1922. The motion of ellipsoidal particles immersed in a viscous fluid. Proceedings of the Royal Society, London 102, 201–211.

Jessell, M.W., 1988. Simulation of fabric development in recrystallizing aggregates: 1. Description of the model. Journal of Structural Geology 10, 771–778.

Jezek, J., 1994. Software for modelling the motion of rigid triaxial ellipsoidal particles in viscous flow. Computers & Geosciences 20, 409–424.

Knipe, R.J., 1989. Deformation mechanisms-recognition from natural tectonites. Journal of Structural Geology 11, 127–146.

Law, R.D., 1990. Crystallographic fabrics: a selective review of their applications to research in structural geology. In: Knipe, R.J., Rutter, E.H. (Eds.), Deformation Mechanisms, Rheology and Tectonics. Geological Society Special Publication 54, pp. 335–352.

Lehner, F.K., 1990. Thermodynamics of rock deformation by pressure solution. In: Barber, D.J., Meredith, P.D. (Eds.), Deformation Processes in Minerals, Ceramics and Rocks. Unwin Hyman, London, pp. 296–333.

Mase, G.E., 1970. Schaum's Outline of Theory and Problems of Continuum Mechanics. McGraw-Hill Book Company, New York.

Passchier, C.W., 1987. Stable positions of rigid objects in non-coaxial flow: a study in vorticity analysis. Journal of Structural Geology 9, 679–690.

Passchier, C.W., 1997. The fabric attractor. Journal of Structural Geology 19, 113–128.

Passchier, C.W., Trouw, R.A.J., 1996. Microtectonics. Springer Verlag, Berlin.

Paterson, M.S., 1973. Thermodynamics and its geological applications. Review of Geophysics and Space Physics 11, 355–389.

Rutter, E.H., 1976. The kinetics of rock deformation by pressure solution. Philosophical Transactions of the Royal Society, London, 203-219.

Sunagawa, I., 1987. Morphology of Crystals. Terra Scientific Publishing Company, Tokyo.

Shimizu, I., 1995. Kinetics of pressure solution creep in quartz: theoretical considerations. Tectonophysics 245, 121–134.

Spiers, C. J., Takeshita, T. (Eds.), 1995. Influence of fluids on deformation processes in rocks, Tectonophysics 245.

Stallard, A., Shelley, D., 1995. Quartz c-axes parallel to stretching directions in very low-grade metamorphic rocks. Tectonophysics 249, 31–40.

Takeshita, T., Hara, I., 1998. c-Axis fabrics and microstructures in a recrystallized quartz vein deformed under fluid-rich greenschist conditions. Journal of Structural Geology 20, 417–431.

Tullis, T.E., 1989. Development of preferred orientation due to anisotropic dissolution/growth rates during solution-transfer creep. EOS Transactions of the AGU 70, 457–458.

Wenk, H.R., 1985. Preferred Orientation in Deformed Metals and Rocks: An Introduction to Modern Texture Analysis. Academic Press Inc, Orlando.